Published in final edited form as:
J Biomed Mater Res A. 2011 September 1; 98(3): 383–393. doi:10.1002/jbm.a.33113.

Adipose tissue-derived stem cells display a proangiogenic phenotype on 3D scaffolds

Evgenios A. Neofytou[1,*], **Edwin Chang**[2,*], **Bhagat Patlola**[1], **Lydia-Marie Joubert**[3], **Jayakumar Rajadas**[4], **Sanjiv S. Gambhir**[2], **Zhen Cheng**[2], **Robert C. Robbins**[1], and **Ramin E. Beygui**[1]

[1]Department of Cardiothoracic Surgery, Stanford University School of Medicine, California

[2]Department of Radiology, Molecular Imaging Program At Stanford, Stanford University School of Medicine, Stanford, California

[3]Cell Sciences Imaging Facility, Stanford University School of Medicine, Stanford, California

[4]Biomaterial and Advance drug delivery Laboratory, Stanford University School of Medicine, Stanford, California

Abstract

Ischemic heart disease is the leading cause of death worldwide. Recent studies suggest that adipose tissue-derived stem cells (ASCs) can be used as a potential source for cardiovascular tissue engineering due to their ability to differentiate along the cardiovascular lineage and to adopt a proangiogenic phenotype. To understand better ASCs' biology, we used a novel 3D culture device. ASCs' and b.END-3 endothelial cell proliferation, migration, and vessel morphogenesis were significantly enhanced compared to 2D culturing techniques. ASCs were isolated from inguinal fat pads of 6-week-old GFP+/BLI+ mice. Early passage ASCs cells (P3-P4), PKH26-labeled murine b.END-3 cells or a co-culture of ASCs and b.END-3 cells were seeded at a density of 1×10^5 on three different surface configurations: (a) a 2D surface of tissue culture plastic, (b) Matrigel, and (c) a highly porous 3D scaffold fabricated from inert polystyrene. VEGF expression, cell proliferation, and tubulization, were assessed using optical microscopy, fluorescence microscopy, 3D confocal microscopy, and SEM imaging ($n = 6$). Increased VEGF levels were seen in conditioned media harvested from co-cultures of ASCs and b.END-3 on either Matrigel or a 3D matrix. Fluorescence, confocal, SEM, bioluminescence revealed improved cell, proliferation, and tubule formation for cells seeded on the 3D polystyrene matrix. Collectively, these data demonstrate that co-culturing ASCs with endothelial cells in a 3D matrix environment enable us to generate prevascularized tissue-engineered constructs. This can potentially help us to surpass the tissue thickness limitations faced by the tissue engineering community today.

Correspondence to: R. E. Beygui; rbeygui@stanford.edu.
*These authors contributed equally to this work.

Additional Supporting Information may be found in the online version of this article.

Author contributions: E.A.N., E.C., R.E.B. and R.C.R. conceived and designed the experiments. E.C., E.A.N. B.P., and L.J. performed the experiments. E.A.N., S.G., J.R., Z.C., R.E.B. and R.C.R., analyzed the data and wrote the paper.

Conflict of interest: None.

Keywords

adipose derived stem cells; neovascularization; tissue engineering; scaffolds

INTRODUCTION

Ischemic heart disease is the leading cause of death worldwide.[1–5] It is characterized by reduced blood flow to the damaged heart muscle followed by death of cardiomyocytes.[6,7] Despite the reduction in mortality rates, as a result of the use of pharmacological agents and percutaneous and surgical coronary intervention, the permanent net loss of contractile cardiac tissue initiates sequelae of congestive heart failure, life threatening arrhythmias, and ultimately death.[8–10] At present, the only curative treatment for end stage congestive cardiac failure is cardiac transplantation with its obvious limitations and complications.[11–14] There is a medical necessity to improve traditional treatments and develop alternatives to current organ transplantation given the worldwide mismatch between patients waiting for transplants and the availability of donor organs as well as infectious and malignant consequences of long-term immunosuppression.

Alternative multidisciplinary approaches, such as the combination of cardiac stem cell therapy with tissue engineering, have attracted considerable attention and expectations.[15–19] One of the fundamental principles of this approach is that the newly formed tissue must maintain its own blood supply to support cellular proliferation, induce structural support and promote tissue regeneration.[20–22] To promote tissue-engineered scaffold vascularization, a number of strategies can be employed. Prominent amongst these strategies is the use of growth factors or cytokines to promote endothelial progenitor cell migration within the engineered construct.[23–25] This has resulted in significant improvement of vascular ingrowth within the newly formed tissue.[24,26] However the short half-life of these growth factors *in vivo*, along with the limited control over their spatial and temporal distribution within the scaffolds, have compelled investigators to seek alternative methods for incorporating vasculature within these engineered constructs.[27,28]

Recently, it has been shown that adipose tissue can be an ideal source for autologous stem cell therapy, since it is easy to obtain from a processed lipo-aspirate and is capable of yielding substantial numbers of adipose tissue-derived stem cells (ASCs) for transplantation.[29–31] Adipose tissue contains an abundant population of stem cells including mesenchymal stem cells and endothelial progenitor cells that under the influence of the appropriate stimuli can differentiate into several lineages,[32] including cardiomyocytes,[33] smooth muscle cells,[32,34] and endothelial cells.[32,35] In addition to this ASCs have been shown to escape immune recognition as they do not express major histocompatibility complex (MHC) class II antigens, thus highlighting their potential to be used in allogeneic transplantations.[36] Under hypoxic conditions such as in the ischemic hind limb model and myocardial infarction models, ASCs have been shown to stimulate blood vessel growth due to their secretion of many angiogenic and anti-apoptotic growth factors.[37,38]

In previous studies, we showed the capability of ASCs to adopt a proangiogenic phenotype on a Matrigel scaffold.[39,40] We also showed the adoption of a similar phenotype for bone-

marrow derived MSCs when they were seeded onto synthetic bone grafts.[41,42] In this study, we aimed to build upon these initial findings and exploit the high proliferative and angiogenic potential of ASCs. To develop *in vitro* proangiogenic tissue structures, we used an approach where undifferentiated ASCs were co-cultured with mouse brain endothelial cells (b.END-3) on an inert highly porous polystyrene scaffold to produce a pre-vascular tube-like tissue constructs. We used b.END-3 cells for these experiments as these cell-lines behave as endothelial cells and are amenable to maintenance and growth in culture media. The b.END-3 cells express von Willebrand factor and uptake fluorescent-labeled low density lipoprotein. We believe this to be the initial steps towards the generation of vascularized tissue engineered constructs that can be used effectively in cardiovascular tissue engineering.

MATERIALS AND METHODS

Basic research design for co-culturing experiments

ASCs were isolated from the inguinal fat pads of BLI and GFP-positive mice as previously described.[43] To make red fluorescent cells, b.END-3 cells were labeled with PKH26 tomato red dye. On day 0, scaffolds were seeded with ASCs and b.END-3 according to the cell seeding protocol described below. Additionally, ASCs and b.END-3 were seeded in polystyrene 2D culture flasks on day 0 (control) and matrigel (positive control). Co-cultures were cultivated for up to 7 days, in which scaffolds were assayed on days 3 and 7 (see Supporting Information Fig. 1). Fully supplemented DMEM containing 10% FBS was used as growth media and was changed every 3 days during the entire duration of the experiments (see Supporting Information Fig. 1).

ASCs harvest and culture

Wild-type C57/BL6 were purchased from Jackson Laboratory (Bar Harbor, ME) and transgenic mice with β-actin promoter driving firefly luciferase and green fluorescent protein (Fluc-GFP) double fusion reporter gene were bred on FVB background. Inguinal fat pads were excised from 6-week-old mice and washed in serial dilutions of Betadine (Purdue Frederick Co., Norwalk, CT). Fat pads were finely minced and the resulting tissue was digested with 0.075% type II collagenase (Sigma-Aldrich, St. Louis, MO) dissolved in Dulbecco's Modified Eagle's Medium, DMEM, (4.5 g/mL glucose; Gibco, Carlsbad, CA,) for 30 min at 37°C. Collagenase was inactivated by adding two volumes of cell culture media (DMEM, 10% fetal bovine serum [FBS], 1% penicillin/streptomycin; Gibco) and the solution was subsequently pelleted to separate mature adipocytes from the remaining stromal-vascular fraction. The supernatant was discarded, and the pellet was re-suspended and filtered through a 100-μm cell strainer to remove undigested tissue fragments. Cells were pelleted, re-suspended in cell culture medium, and plated at 3×10^6 cells per 100 cm^2 culture plate. Fully supplemented DMEM (Gibco, Carlsbad, CA) containing 10% FBS 1% penicillin/streptomycin; (Gibco) was used as growth media, it was changed 24 h after the initial plating and every 3 days thereafter. ASCs were allowed to grow to sub-confluence before detachment using 0.25% trypsin-ethylenediaminete-traacetic acid (Sigma-Aldrich). Early passage cells (P3-P4) were used in all experiments as specified below.

Animal care was provided in accordance with the Stanford University School of Medicine guidelines and policies for the use of laboratory animals. All protocols were approved by the Administrative Panel on Laboratory Animal Care at the Stanford University School of Medicine.

PKH26 fluorescent labeling

The b.END-3 cells were labeled with the fluorescent dye PKH26 (MINI26 cell linker kit, Sigma-Aldrich), which is a lipophilic fluorescent that binds irreversibly to the cell membrane and is not transferable to other cells. The cells were prepared according to the manufacturer (Sigma). Briefly, the cells were re-suspended in a concentration of 10^7 cells/mL, followed by the addition of fluorescent dye PKH26 to a final concentration of 2×10^6 *M*. Two minutes later the reaction was stopped by addition of fetal bovine serum. Finally, cells were washed three times with the medium and finally re-suspended in fully supplemented DMEM containing 10% FBS cell medium. Onto 3D membranes, 1×10^5 cells were seeded immediately and cultured at 37°C with 5% CO_2.

Structure of Alvetex® 3D polystyrene scaffolds

The Alvetex® 3D polystyrene scaffolds were purchased from Reinnervate (Durham, UK). The scaffolds were developed using emulsion template technique to control the size of the highly interconnected pores ~40 μm in size [Fig. 1(e)]. These thin microcellular scaffolds were initially cast as a monolith and subsequently sliced into 200 μm thick membranes [Fig. 1(b)]. The highly porous thin membrane enabled cells to proliferate within the membranes as wells as allowing for sufficient mass exchange of gases, nutrients, and waste products during the *in vitro* cell culture process. The 3D geometry of the scaffold provides the environment in which cells grow, differentiate, and proliferate to form close relationships with their adjacent cells. This gave us the opportunity to create constructs that are equivalent to a thin tissue layer *in vitro*. The 3D scaffolds used were made from inert polystyrene and were treated in the same manner as traditional 2D cell culture plastic vessels used for the control experiments.

Cell seeding

Sterilized membranes were placed into 6-well tissue culture plates and seeded with (1×10^5 cells ASCs, b.END-3), or a combination of (0.5×10^5 ASCs and 0.5×10^5 b.END-3). The cell suspension was pipetted directly onto the top center surface of the membrane scaffolds. Cells were allowed to attach to scaffolds for 1 h before addition of 2 mL of medium (Fully supplemented DMEM containing 10% FBS) into each well. Cells were maintained in a humidified incubator at 37°C with 5% CO_2 for the duration of the experiments.

Scanning electron microscopy (SEM)

SEM was performed on scaffolds with and without cells to investigate scaffold and cell morphology. Samples were fixed with 4% Paraformaldehyde and 2% Glutaraldehyde in 0.1 *M* sodium cacodylate buffer (pH 7.3) (EMS, Hatfield, PA). After rinsing in the same buffer, samples were post-fixed in 1% aqueous OsO_4 (1 h), and thereafter visualized fully hydrated with a Hitachi S-3400N Variable Pressure SEM (Hitachi High-Tech, Japan) operated at 50–

60 Pa chamber pressure, WD 5–7 mm, and 15 kV accelerating voltage. Moisture loss was controlled with a Deben Coolstage (Deben UK Ltd, Suffolk, UK) by decreasing temperature to −25°C at 60 Pa V.

Matrigel tubule assay

Matrigel (BD Biosciences) was thawed and placed in four-well chamber slides at 37°C for 30 min to allow solidification. GFP^+ ASCs (passage 3) at 1×10^5 were plated alone on Matrigel and incubated at 37°C under normoxic conditions for 72 h. GFP^+ ASCs at 0.5×10^5 were also co-plated with 0.5×10^5 PKH26-labeled murine b.END-3 endothelial cells (American Type Culture Collection, Manassas, VA) on Matrigel and incubated under the same conditions. This assay was repeated using 1×10^5 PKH26-labeled murine b.END-3 endothelial cells plated alone (control), as above. The alignment of endothelial cells and the generation of a patent lumen were consider as tubule formation, and was defined as a structure exhibiting a length four times its width. Experiments were performed with $n = 6$ and was quantified in five random 10 × fields by two blinded observers.

Quantification of the number of viable cells by bioluminescence assay

To eliminate the difference in the level of luciferase expression in each cell line, calibration of photon flux with respect to actual cell count was performed. ASCs were dislodged from culture flasks and re-suspended in in 100 μL of DMEM were seeded into a 96 well plate by serial dilutions in known concentrations per well, each repeated with three independent experiments. After administration of D-luciferin, (Xenogen, Alameda, CA, 4.5 ug/mL). The plate was imaged using the IVIS 100 system (2 min, 8 bin, and level B/FOV 15 × 15 cm) (Xenogen Corporation, Alameda, CA) at 10 min after addition of luciferin at the final concentration of 150 μg/mL. DMEM media without luciferin were served as negative control. The photon flux was linearly regressed on the actual cell count to obtain a calibration curve for each cell line, as previously reported. Peak signal (photons/second/square centimeter/steridian or $p/s/cm^2/sr$) was measured using a charged coupled device camera (IVS200, Xenogen, Alameda, CA).

The baseline of the ASCs proliferation was obtained by BLI assay 12 h after cells were planted. Lights emitted from ASCs cells were acquired until 3 days post seeding of the cells on the three different culture surfaces. Averages of three kinetic bioluminescent acquisitions were obtained within 10 min for each acquisition time point. Regions of interest were drawn over wells automatically and quantified by Living Image Software version 2.20. Data were analyzed based on total photon flux emission (photons/s) subtracted by the background photon flux of each well for the dark current measurement.

Confocal microscopy

Cell organization on the 3D membrane scaffolds was characterized via confocal microscopy on day 7. Confocal microscopy was performed using a Leica TCS SP2 AOBS confocal system. Three-dimensional confocal images were generated from individual slices using high-resolution opacity rendering. Fluorescence microscopy was performed with a Leica DMI4000 B microscope. GFP-labeled ASCs were detected via 483/520 (ex/em), and PKH26

tomato red-labeled b.END-3 were detected at 483/600 (ex/em). All confocal imaging was completed at the Cell Sciences Imaging Facility at Stanford University.

VEGF enzyme-linked immunosorbent assay

The collected cell culture supernatants, conditioned medium was obtained from the nine different groups cultured at normal oxygen tension conditions. VEGF levels were assayed using a Quantikine murine VEGF enzyme-linked immunosorbent assay (ELISA) kit (R&D Systems, Minneapolis, MN,) in accordance with the manufacturer's protocol. Results were reported in nanograms per milliliter and experiments were performed in triplicate with $n = 3$ and normalized it to the initial cell number.

Statistical analysis

Results are presented as mean ± standard error of the mean. Data analysis was performed using the Student's *t*-test [Matrigel, migration, endothelial differentiation, or one-way analysis of variance (VEGF ELISA and proliferation studies)]. Results were considered significant at $p < 0.05$. Data were analyzed with Prism software (GraphPad Software, La Jolla, CA, http://www.graphpad.com).

RESULTS

ASCs form a capillary-like network when co-cultured with b.END-3 *in Vitro* on 3D scaffolds

ASCs are abundant in tissues that are rich with vasculature, thereby suggesting that the presence of ASCs furnishes a proangiogenic environment.[44,45] Thus, we were interested to test whether ASCs have the potential to form tubular structures. In an *in vitro* tubule formation assay, ASCs were co-cultured with b.END-3 endothelial cells onto either a 2D surface scaffold [Fig. 3I(a–i)] Matrigel [Fig. 3II(a)]or a 3D polystyrene membrane scaffolds [Fig. 4(a–f)]. On the 3D scaffold, seeding with only b.END-3 or ASCs resulted in either an absence of, or minimal tubule formation [Fig. 2(a,b)]. However, by seeding a mixed culture of b.END-3 with ASCs onto Matrigel, a prominent tubular network was produced [Figs. 2(d) and 3II(a)]. The ability of both cell types to interact with each other to form a proangiogenic tubular network is illustrated in [Figs. 3I and 4(a–f)]. Such findings are consistent with and extend upon our previous findings whereby interactions between endothelial cells and mesenchymal stem cell types created enhanced tubular networks on either Matrigel[40] or on artificial bone grafts.[42]

Adipose-derived sromal cells and endothelial cells polarize around the porous depressions of the 3D scaffolds

To determine if a similar cooperation exists on novel 3D membrane scaffolds, co-cultures were also performed on Matrigel [Fig. 2(a–c)] and 3D polystyrene [Fig. 2(e–g)]. Scanning Electron Micrographs (SEM) showed that when seeded alone onto Matrigel, b.END-3 produced a poorly defined microvillus network [Fig. 2(a)] while ASCs produced none at all since they formed a multi-layered cell sheet [Fig. 2(b)]. This observation also held for single seeding of b.END-3 cells or ASCs onto 3D polystyrene scaffolds [Fig. 2(e,f)].However, when b.END-3 and ASCs were seeded together onto either Matrigel or 3D membrane

scaffolds, there was a markedly increased frequency of complex microvillus and tubulogenic networks compared to the 2D polystyrene culture dishes[Figs. 2(c,g), 3II and 4(a–f)].

In addition to this, there were important qualitative differences in the networks produced in Matrigel versus those produced in the 3D scaffolds. For cells seeded onto Matrigel, a typical tubulogenic network was observed across the field of view of the pictograph [Fig. 3II(a)]. But for 3D scaffolds the ASCs tended to congregate and polarize around porous depressions of the substrate and create a complex latticelike pattern of microvilli acting as a collective anchorage network with an enhanced surface area interfacing with the substrate and the b.END-3 endothelial cells [Figs. 3II(b) and 4(a,b)]. The extent of cellular interaction as a portion of scaffold surface seemed to be greater for cells on 3D scaffolds than those on Matrigel. When cells are mixed together on 2D surfaces, b.End-3 formed clumps and ASCs formed tubules around them preventing them from becoming confluent [Fig. 3I(g–i)].These regions were not observed among control ASCs seeded onto 2D surfaces when maintained under identical culture conditions [Fig. 3I(a–f)].

SEM imaging of ASCs and b.END-3 cells seeded onto the 3D scaffolds in co-culture was performed in cross-section, the presence of both cell types beneath the outer surface of scaffolds was observed as seen on a representative image of scaffold shown in [Fig. 2(g,h)]. Although the images obtained were purely qualitative, they demonstrated that both cell types proliferate and self-organize within the internal porous structure of the 3D polystyrene scaffolds as seen by confocal microscopic images.

Confocal microscopy of ASCs and b.END-3 structures

Cell fate was analyzed at 7 days after cell seeding by fluorescent microscopy against GFP+ ASCs. Green fluorescence was easily detected along the cell surface membranes of the newly formed tissue constructs. Confocal microscopy images [Fig. 4(b–f)] confirmed that ASCs and b.END-3 cells were able to penetrate the outer surface of the scaffolds and migrate towards the internal interconnected porous structure [Fig. 6(a–h)]. Taken together, these findings indicate that GFP-expressing ASCs do interact with the PKH2 labeled b.END-3 producing a proangiogenic environment.

Increased expression of Luciferase in ASCs and b.END-3 co-cultures on matrigel, and 3D scaffolds membranes

To quantify the cell proliferation based on the detected photons from the living cells, we have determined the correlation between the number of ASCs and the expression levels of luciferase using BLI assay [Fig. 4(c,d)]. In our experiments we have shown that when cells were mixed together, using Matrigel as a seeding surface, b.End-3 cells formed clumps while the ASCs formed tubules around them thus preventing them from becoming confluent. This is also indicated by the BLI signal of this co-culture being much lower than when these two cell types are co-cultured together within the 3D membrane scaffolds [Fig. 4(a,b)]. The 3D membrane scaffolds provided a more efficient support for the growth and proliferation of both b.END-3 and ASCs [Fig. 4(a,b)]. Cell cultures became more confluent than comparable Matrigel matrices. We hypothesize that this observation is a result of the 3D geometry of the

scaffolds that can allow the cells to form close relationships with each other as seen in an *in vivo* setting.

Adoption of proangiogenic phenotype by ASCs, and the release of angiogenic cytokines

Angiogenesis is a complex phenomenon, which includes the formation of new blood vessels by capillary sprouting from pre-existing vessels. ASCs possess not only the ability to differentiate into multiple cell types but also contribute to tissue regeneration through expressing many hematopoietic and angiogenic cytokines.[46–48] A prominent example is vascular endothelial growth factor (VEGF) the most effective and specific growth factor that regulate angiogenesis.[47,49] We sought to clarify the impact on VEGF expression by ASCs, specifically examining the influence of varying surfaces on VEGF secretion. ASCs and b.End-3 increase the VEGF expression progressively under Matrigel and 3D scaffold area in culture [Fig. 7(b,c)]. Furthermore, we found a significantly elevated secretion of VEGF (3.5 fold increase, $p < 0.0412$) within the supernatant media of the co-cultures seeded on Matrigel [Fig. 5(b)] and 3D scaffold ($p < 0.028$), when compared with co-cultures seeded on the 2D control culture plates [Fig. 7(a)] as quantified by ELISA.

DISCUSSION

The salient findings from these studies are these: (1) co-seeding of ASCs with endothelial cells onto a 2D or 3D polystyrene scaffolds resulted in the formation of a tubulogenic network more elaborate than that of single cell type seeding, (2) The 3D architecture of membrane scaffolds also drives patterning of the seeded cells to a protubulogenic environment that increases the release of angiogenic cytokines as seen by the increase in VEGF release, and (3) seeding onto different surfaces 2D, 3D, and Matrigel has differential functional consequences on co-culturing the two cell types together. These findings are consistent with previous studies[39,40] that our group has published where we showed an intrinsic co-operability between mesenchymal derived stem cells (such as ASCs) and endothelial cells forming prevascular networks when seeded together.[40]

The enhancement of tubulogenic network formation with co-seeding of mesenchymal type stem cells and endothelial cells onto Matrigel or on Ca^{+}-Phosphate based artificial bone grafts a 3D matrix has been well described in the literature.[39–41,50] Our report extends upon these studies by comparing the network forming capacities of Matrigel to 2D and 3D polystyrene surfaces. Interestingly, such a co-seeding onto plastic 2D polystyrene culture plates failed to produce any cellular organization reminiscent of a tubulogenic or microvillus network.

The data presented in this report illustrate that thus far three known factors contribute to effective tubulogenesis *in vitro:* (a) the angiogenic factors that are produced by the participating cell types, (for our studies, the ASCs), (b) the physical interaction of vascular and stem cells to provide a competent, protubulogenic environment, and (c) the structure and architecture of the underlying scaffolds that somehow enhance and support the interaction of cells to form tubules.

ASC share several phenotypic and functional similarities with mesenchymal cells which can undergo a proangiogenic conversion under hypoxic conditions.[40] Those same mesenchymal-derived cells secrete VEGF when cultured under low oxygen conditions. Bone marrow-derived MSCs can be coaxed into secreting VEGF and SDF-1α when either interacting with endothelial cells[40] or by being seeded onto various artificial bone grafts.[41] In our present studies, the ASCs behaved in a similar manner whereby the stem cells secreted VEGF when stimulated by interaction with b.END-3 along with seeding on top of 2D and 3D scaffolds. Taken together our present and previous studies illustrate that adipose tissue-derived stem cells become involved in organogenesis through environment-dependent induction of cytokines such as VEGF[41] The "activation" of stem or differentiated cells through alterations in interaction with other stromal cell types is not unprecedented. For instance, quiescent hematopoietic stem cells (HSCs) are attached to a bed of stromal "niche" cells within the bone marrow through surface expression of the c-Kit ligand (SCF) that binds to c-Kit receptors (CD117) of niche cells. Systemic signaling that prompts HSC mobilization (such as a challenge with GM-CSF) leads to expression of soluble matrix metalloproteinase (MMP9) that results in cleavage of the sKit ligand and subsequent detachment of HSCs from the niche bed. Eventually the HSCs are delivered into the circulation[51,52] When challenged with Matrigel, endothelial cells begin to express the integrin $\alpha_v\beta_3$ whose function in this situation is to promote cell-to-cell adhesion and tubule formation.[53,54] The cells failing to adhere to one another through $\alpha_v\beta_3$-mediated adhesion will eventually undergo apoptosis[53] and die. We speculate that mutual interaction of endothelial cells with ASCs (perhaps analogous to stem cell/niche cell interactions) results in induction of cytokines conducive to tubule formation. In fact, several groups are actively exploring the behavior of ASCs *in vivo* or ex vivo when they interact with putative adipose niche environments.[55,56]

There may be qualitative differences in the manner in which the cells behave on different scaffolds. For instance, Matrigel provides an appropriate topological and cytokine environment for efficient capillary-like formation. However, Matrigel lacks the porous qualities that are intrinsic to the 3D polystyrene scaffolds. The 3D scaffolds are characterized by high porosity (>90%) with an average pore size of 35–45 μm in diameter and high degree of pore interconnectivity. With such features, seeded cells can efficiently migrate deeply into the scaffold when compared to the relatively dense matrix of Matrigel. These matrix properties should enable the penetration of these proangiogenic tubules into our 3D scaffolds and allow their efficient vascularization after implantation. The greater latitude for migration affords greater space for enhanced interaction, remodeling and proliferation between the ASCs and b.END-3 cells. One consequence of this would be the enhanced cellular density of seeded 3D scaffolds, which in turn is reflected in an augmented production of angiogenic cytokines such as VEGF [Fig. 7(c)]. The impact of differences in matrix porosity and topology on organization and functionality of the constructs has been shown before on artificial bone grafts,.[50] In studies by Roldan et al., it was showed that the seeding of same numbers of MSCs onto several types of bone grafts that differ in their bone composition, porosity, and permeability yielded strikingly different results in terms of downstream cytokine productions such as VEGF and SDF-l-α.[50]

In conclusion, this work represents the culmination of a series of experiments in which we explore the contributions of cellular composition of differentiated cells versus stem cells as well as the contribution of different surfaces such as 2D, 3D, and Matrigel to better understand the cell biology and cell-cell interactions that are required to more closely represent the natural structure and function of tissues seen in the *in vivo* setting. Our findings revealed the strong influence of matrix porosity in driving ASCs and endothelial cell interaction thus providing an environment that significantly enhances the functional activity of cells when compared with cells grown on 2D culture plates. Our work shows ASCs co-cultured with endothelial cells on porous 3D scaffolds allow formation of complex tubular structures that morphologically resemble pre-vascularized constructs. Matrigel, which is secreted from the mouse sarcomatous cells, contains growth factors and various peptides and proteins. In lieu of Matrigel, carefully designed 3D scaffolds with known composition can potentially help us solve some of the challenges faced by the tissue engineering community today. These results could be the initial steps to help us design a complex 3D organ by promoting cell differentiation, vessel formation, and cell survival within a 3D tissue engineered construct. Our future experiments will address construction of 3D scaffolds that are biocompatible and implantable. Such insights will be invaluable in building upon our current expertise and capabilities towards viable and effective tissue bioengineering.

Supplementary Material

Refer to Web version on PubMed Central for supplementary material.

Acknowledgments

Contract grant sponsor: Stanford School of Medicine

Contract grant sponsor: American Heart Association; contract grant number: 11IRG5450017

Contract grant sponsor: NCI ICMIC; contract grant number: P50CA114747

REFERENCES

1. Murray CJ, Lopez AD. Mortality by cause for eight regions of the world: Global burden of disease study. Lancet. 1997; 349:1269–1276. [PubMed: 9142060]
2. Heron M, Hoyert DL, Murphy SL, Xu J, Kochanek KD, Tejada-Vera B. Deaths: Final data for 2006. Natl Vital Stat Rep. 2009; 57:1–134. [PubMed: 19788058]
3. Minino AM, Heron MP, Murphy SL, Kochanek KD. Deaths: Final data for 2004. Natl Vital Stat Rep. 2007; 55:1–119. [PubMed: 17867520]
4. Kung HC, Hoyert DL, Xu J, Murphy SL. Deaths: Final data for 2005. Natl Vital Stat Rep. 2008; 56:1–120. [PubMed: 18512336]
5. Stewart S, Maclntyre K, Hole DJ, Capewell S, McMurray JJ. More 'malignant' than cancer? Five-year survival following a first admission for heart failure. Eur J Heart Fail. 2001; 3:315–322. [PubMed: 11378002]
6. Ferrari R, Ceconi C, Campo G, Cangiano E, Cavazza C, Secchiero P, Tavazzi L. Mechanisms of remodelling: a question of life (stem cell production) and death (myocyte apoptosis). Circ J. 2009; 73:1973–1982. [PubMed: 19822975]
7. Frantz S, Bauersachs J, Ertl G. Post-infarct remodelling: Contribution of wound healing and inflammation. Cardiovasc Res. 2009; 81:474–481. [PubMed: 18977766]

8. Wexler RK, Elton T, Pleister A, Feldman D. Cardiomyopathy: An overview. Am Fam Physician. 2009; 79:778–784. [PubMed: 20141097]
9. Deedwania PC, Lardizabal JA. Atrial fibrillation in heart failure: A comprehensive review. Am J Med. 2010; 123:198–204. [PubMed: 20193823]
10. Cleland JG. Progression from hypertension to heart failure. Mechanisms and management. Cardiology. 1999; 92(Suppl 1):10–19. discussion 20–21. [PubMed: 10652967]
11. Miniati DN, Robbins RC. Heart transplantation: A thirty-year perspective. Annu Rev Med. 2002; 53:189–205. [PubMed: 11818470]
12. Ogata K, Platt JL. Cardiac xenotransplantation: Future and limitations. Cardiology. 2004; 101:144–155. [PubMed: 14988636]
13. Massad MG. Current trends in heart transplantation. Cardiology. 2004; 101:79–92. [PubMed: 14988629]
14. Korewicki J. Cardiac transplantation is still the method of choice in the treatment of patients with severe heart failure. Cardiol J. 2009; 16:493–499. [PubMed: 19950084]
15. Chien KR, Domian IJ, Parker KK. Cardiogenesis and the complex biology of regenerative cardiovascular medicine. Science. 2008; 322:1494–1497. [PubMed: 19056974]
16. Jawad H, Ali NN, Lyon AR, Chen QZ, Harding SE, Boccaccini AR. Myocardial tissue engineering: a review. J Tissue Eng Regen Med. 2007; 1:327–342. [PubMed: 18038427]
17. Christman KL, Lee RJ. Biomaterials for the treatment of myocardial infarction. J Am Coll Cardiol. 2006; 48:907–913. [PubMed: 16949479]
18. Zimmermann WH, Eschenhagen T. Cardiac tissue engineering for replacement therapy. Heart Fail Rev. 2003; 8:259–269. [PubMed: 12878835]
19. Wu KH, Cui B, Yu CT, Liu YL. Stem cells: New cell source for myocardial constructs tissue engineering. Med Hypotheses. 2006; 67:1326–1329. [PubMed: 16814940]
20. Melero-Martin JM, De Obaldia ME, Kang SY, Khan ZA, Yuan L, Oettgen P, Bischoff J. Engineering robust and functional vascular networks in vivo with human adult and cord blood-derived progenitor cells. Circ Res. 2008; 103:194–202. [PubMed: 18556575]
21. Traktuev DO, Prater DN, Merfeld-Clauss S, Sanjeevaiah AR, Saadatzadeh MR, Murphy M, Johnstone BH, Ingram DA, March KL. Robust functional vascular network formation in vivo by cooperation of adipose progenitor and endothelial cells. Circ Res. 2009; 104:1410–1420. [PubMed: 19443841]
22. Jain RK, Au P, Tam J, Duda DG, Fukumura D. Engineering vascularized tissue. Nat Biotechnol. 2005; 23:821–823. [PubMed: 16003365]
23. Nourse MB, Halpin DE, Scatena M, Mortisen DJ, Tulloch NL, Hauch KD, Torok-Storb B, Ratner BD, Pabon L, Murry CE. VEGF induces differentiation of functional endothelium from human embryonic stem cells: implications for tissue engineering. Arte-rioscler Thromb Vase Biol. 2010; 30:80–89.
24. Santos MI, Reis RL. Vascularization in bone tissue engineering: Physiology, current strategies, major hurdles and future challenges. Macromol Biosci. 2010; 10:12–27. [PubMed: 19688722]
25. Zisch AH, Lutolf MP, Hubbell JA. Biopolymeric delivery matrices for angiogenic growth factors. Cardiovasc Pathol. 2003; 12:295–310. [PubMed: 14630296]
26. Soker S, Machado M, Atala A. Systems for therapeutic angiogenesis in tissue engineering. World J Urol. 2000; 18:10–18. [PubMed: 10766038]
27. Lesman A, Habib M, Caspi O, Gepstein A, Arbel G, Levenberg S, Gepstein L. Transplantation of a tissue-engineered human vascuarized cardiac muscle. Tissue Eng Part A. 2010; 16:115–125. [PubMed: 19642856]
28. Kalka C, Asahara T, Krone W, Isner JM. [Angiogenesis vascuogenesis. Therapeutic strategies for stimulation of postnatal neovascularization]. Herz. 2000; 25:611–622. [PubMed: 11076319]
29. Brayfield C, Marra K, Rubin JP. Adipose stem cells for soft tissue regeneration. Handchir Mikrochir Plast Chir. 2010; 42:124–128. [PubMed: 20352575]
30. Cherubino M, Marra KG. Adipose-derived stem cells for soft tissue reconstruction. Regen Med. 2009; 4:109–117. [PubMed: 19105620]

31. Sandor GK, Suuronen R. Combining adipose-derived stem cells, resorbable scaffolds and growth factors: An overview of tissue engineering. J Can Dent Assoc. 2008; 74:167–170. [PubMed: 18353203]
32. Madonna R, De Caterina R. Adipose tissue: A new source for cardiovascular repair. J Cardiovasc Med (Hagerstown). 2010; 11:71–80. [PubMed: 19996982]
33. Choi YS, Dusting GJ, Stubbs S, Arunothayaraj S, Han XL, Collas P, Morrison WA, Dilley RJ. Differentiation of human adipose-derived stem cells into beating cardiomyocytes. J Cell Mol Med. 2010; 14:878–889. [PubMed: 20070436]
34. Wang C, Yin S, Cen L, Liu Q, Liu W, Cao Y, Cui L. Differentiation of adipose-derived stem cells into contractile smooth muscle cells induced by transforming growth factor-betal and bone morphogenetic protein-4. Tissue Eng Part A. 2010; 16:1201–1213. [PubMed: 19895205]
35. Cao Y, Meng Y, Sun Z, Liao LM, Han Q, Li J, Liu YN, Zhao CH. [Potential of human adipose tissue derived adult stem cells differentiate into endothelial cells]. Zhongguo Yi Xue Ke Xue Yuan Xue Bao. 2005; 27:678–682. [PubMed: 16447636]
36. Mcintosh KR, Lopez MJ, Borneman JN, Spencer ND, Anderson PA, Gimble JM. Immunogenicity of allogeneic adipose-derived stem cells in a rat spinal fusion model. Tissue Eng Part A. 2009; 15:2677–2686. [PubMed: 19207041]
37. Kang JH, Gimble JM, Kaplan DL. In vitro 3D model for human vascularized adipose tissue. Tissue Eng Part A. 2009; 15:2227–2236. [PubMed: 19207036]
38. Verseijden F, Jahr H, Posthumus-van Sluijs SJ, Ten Hagen TL, Hovius SE, Seynhaeve AL, van Neck JW, van Osch GJ, Hofer SO. Angiogenic capacity of human adipose-derived stromal cells during adipogenic differentiation: An in vitro study. Tissue Eng Part A. 2009; 15:445–452. [PubMed: 18652540]
39. Hamou C, Callaghan MJ, Thangarajah H, Chang E, Chang El, Grogan RH, Paterno J, Vial IN, Jazayeri L, Gurtner GC. Mesenchymal stem cells can participate in ischemic neovascularization. Plast Reconstr Surg. 2009; 123(2 Suppl):45S–55S. [PubMed: 19182663]
40. Thangarajah H, Vial IN, Chang E, El-Ftesi S, Januszyk M, Chang El, Paterno J, Neofytou E, Longaker MT, Gurtner GC. IFATS collection: Adipose stromal cells adopt a proangiogenic phenotype under the influence of hypoxia. Stem Cells. 2009; 27:266–274. [PubMed: 18974212]
41. Roldan JC, Chang E, Kelantan M, Jazayeri L, Deisinger U, Detsch R, Reichert TE, Gurtner GC. Quantifying migration and polarization of murine mesenchymal stem cells on different bone substitutes by confocal laser scanning microscopy. J Craniomaxillofac Surg. 2010; 38:580–588. [PubMed: 20189818]
42. Roldan JC, Detsch R, Schaefer S, Chang E, Kelantan M, Waiss W, Reichert TE, Gurtner GC, Deisinger U. Bone formation and degradation of a highly porous biphasic calcium phosphate ceramic in presence of BMP-7, VEGF and mesenchymal stem cells in an ectopic mouse model. J Craniomaxillofac Surg. 2010; 38:423–430. [PubMed: 20189819]
43. van der Bogt KE, Schrepfer S, Yu J, Sheikh AY, Hoyt G, Govaert JA, Velotta JB, Contag CH, Robbins RC, Wu JC. Comparison of transplantation of adipose tissue-and bone marrow-derived mesenchymal stem cells in the infarcted heart. Transplantation. 2009; 87:642–652. [PubMed: 19295307]
44. Cho HH, Kim YJ, Kim JT, Song JS, Shin KK, Bae YC, Jung JS. The role of chemokines in proangiogenic action induced by human adipose tissue-derived mesenchymal stem cells in the murine model of hindlimb ischemia. Cell Physiol Biochem. 2009; 24:511–518. [PubMed: 19910691]
45. Kim Y, Kim H, Cho H, Bae Y, Suh K, Jung J. Direct comparison of human mesenchymal stem cells derived from adipose tissues and bone marrow in mediating neovascularization in response to vascular ischemia. Cell Physiol Biochem. 2007; 20:867–876. [PubMed: 17982269]
46. Schenke-Layland K, Strem BM, Jordan MC, Deemedio MT, Hedrick MH, Roos KP, Fraser JK, Maclellan WR. Adipose tissue-derived cells improve cardiac function following myocardia infarction. J Surg Res. 2009; 153:217–223. [PubMed: 18694573]
47. Murohara T, Shintani S, Kondo K. Autologous adipose-derived regenerative cells for therapeutic angiogenesis. Curr Pharm Des. 2009; 15:2784–2790. [PubMed: 19689349]

48. Kilroy GE, Foster SJ, Wu X, Ruiz J, Sherwood S, Heifetz A, Ludlow JW, Stricker DM, Potiny S, Green P, Halvorsen YD, Cheatham B, Storms RW, Gimble JM. Cytokine profile of human adipose-derived stem cells: Expression of angiogenic, hematopoietic, and pro-inflammatory factors. J Cell Physiol. 2007; 212:702–709. [PubMed: 17477371]

49. Li J, Brown LF, Hibberd MG, Grossman JD, Morgan JP, Simons M. VEGF, flk-1, and flt-1 expression in a rat myocardial infarction mode of angiogenesis. Am J Physiol. 1996; 270(5 Pt2):H1803–H1811. [PubMed: 8928889]

50. Roldan JC, Detsch R, Schaefer S, Chang E, Kelantan M, Waiss W, Reichert TE, Gurtner GC, Deisinger U. Bone formation and degradation of a highly porous biphasic calcium phosphate ceramic in presence of BMP-7. VEGF and mesenchymal stem cells in an ectopic mouse model. J Craniomaxillofac Surg. 2010; 38:423–430. [PubMed: 20189819]

51. Kopp HG, Avecilla ST, Hooper AT, Rafii S. The bone marrow vascular niche: home of HSC differentiation and mobilization. Physiology (Bethesda). 2005; 20:349–356. [PubMed: 16174874]

52. Heissig B, Ohki Y, Sato Y, Rafii S, Werb Z, Hattori K. A role for niches in hematopoietic cell development. Hematology. 2005; 10:247–253. [PubMed: 16019473]

53. Arnaoutova I, George J, Kleinman HK, Benton G. The endothelial cell tube formation assay on basement membrane turns 20: State of the science and the art. Angiogenesis. 2009; 12:267–274. [PubMed: 19399631]

54. Eliceiri BP, Cheresh DA. Role of alpha v integrins during angiogenesis. Cancer J. 2000; 6(Suppl 3):S245–S249. [PubMed: 10874494]

55. Yang, Yl; Kim, HI.; Choi, MY.; Son, SH.; Seo, MJ.; Seo, JY.; Jang, WH.; Youn, YC.; Choi, KJ.; Cheong, SH.; Shelby, J. Ex vivo organ culture of adipose tissue for in situ mobilization of adipose-derived stem cells and defining the stem cell niche. J Cell Physiol. 2010; 224:807–816. [PubMed: 20578248]

56. Rajashekhar G, Traktuev DO, Roell WC, Johnstone BH, Merfeld-Clauss S, Van Natta B, Rosen ED, March KL, Clauss M. IFATS collection: Adipose stromal cell differentiation is reduced by endothelial cell contact and paracrine communication: Role of canonical Wnt signaling. Stem Cells. 2008; 26:2674–2681. [PubMed: 18669909]

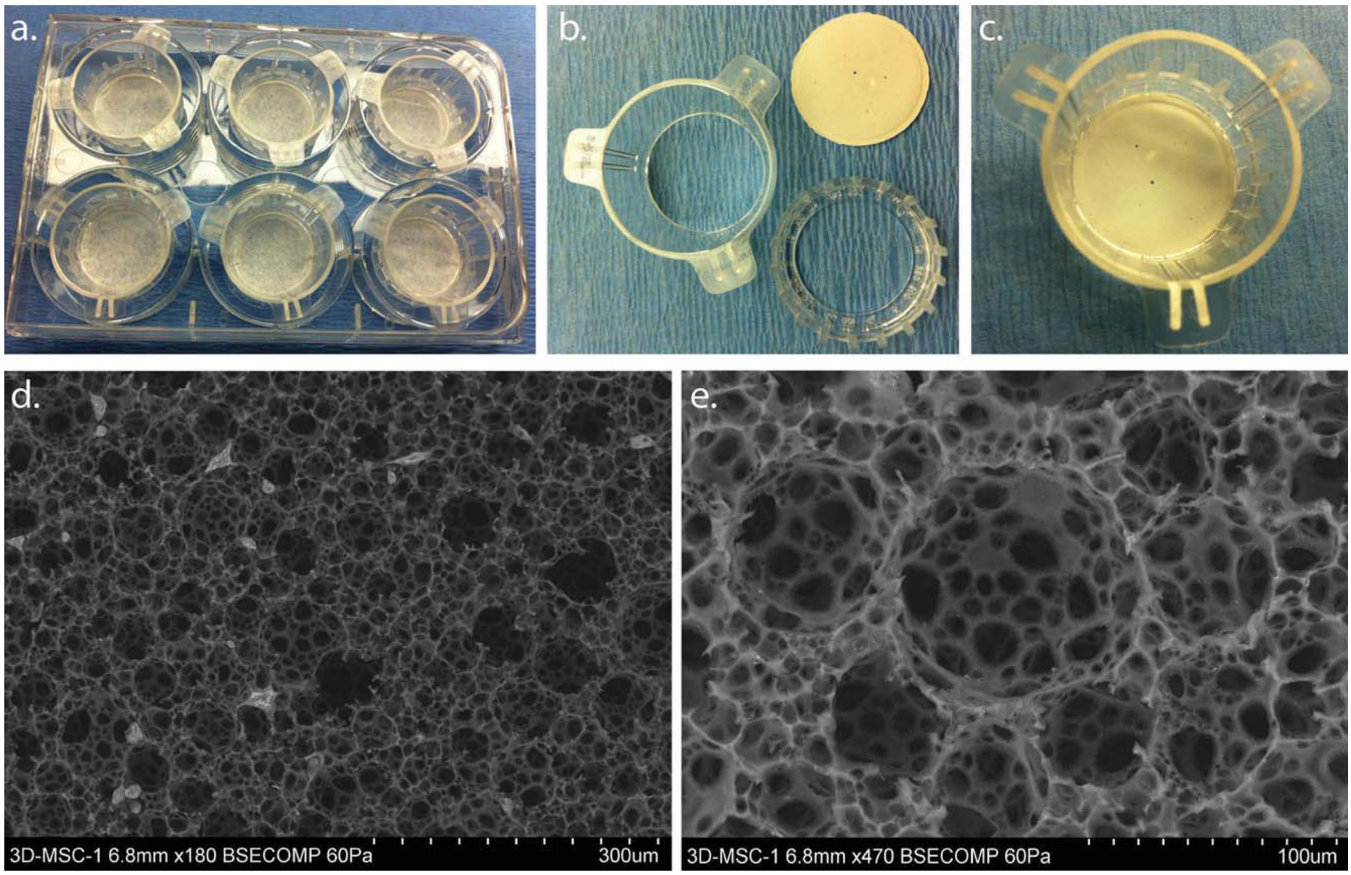

FIGURE 1.

Polystyrene three dimensional (3D) cell culture devices are supplied in a variety of multi-welled plates. A 6-well plate example is shown with 3D cell culture well inserts in (a). The well insert consists of a two-part assembly that fits together to clamp the ~200 μm thick scaffolds in position (b). The well insert can accommodate larger medium volumes to support long-term 3D cell culture (c). The structure of this 3D cell culture substrate consists of a highly porous polystyrene scaffold. SEM show the structural characteristics of the 3D scaffolds at low (d), and high magnifications, see scale bar insert (e). [Color figure can be viewed in the online issue, which is available at wileyonlinelibrary.com.]

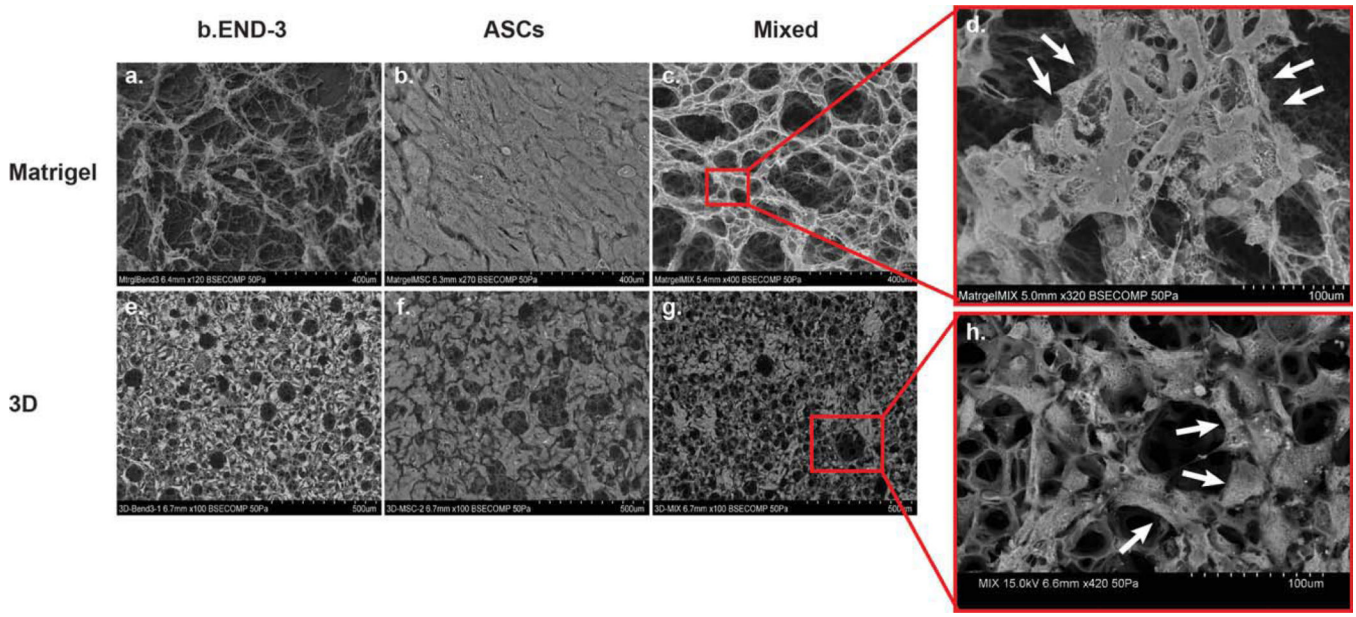

FIGURE 2.

SEM depicting organization and proliferation of ASCs, and b.END-3 cells when co-cultured or seeded alone on Matrigel and 3D polystyrene substrate (a–h). Scanning electron micrograph showing the multi-layered growth of ASCs (b and f) on both cultured surfaces. A construct made with ASCs, and b.END-3 cells, demonstrates the porous structure of the 3D scaffold (g). High-magnification image of a scaffold seeded with a ASCs, and b.END-3 cells, that demonstrate homogeneous and complete cellular distribution throughout the porous surfaces of the scaffold (h). The cells polarize around the pore (indicated by arrows) in a similar fashion as the one seen during the formation of branching, tubular structures (indicated by arrows developed *in vitro* in Matrigel (c and d). [Color figure can be viewed in the online issue, which is available at wileyonlinelibrary.com.]

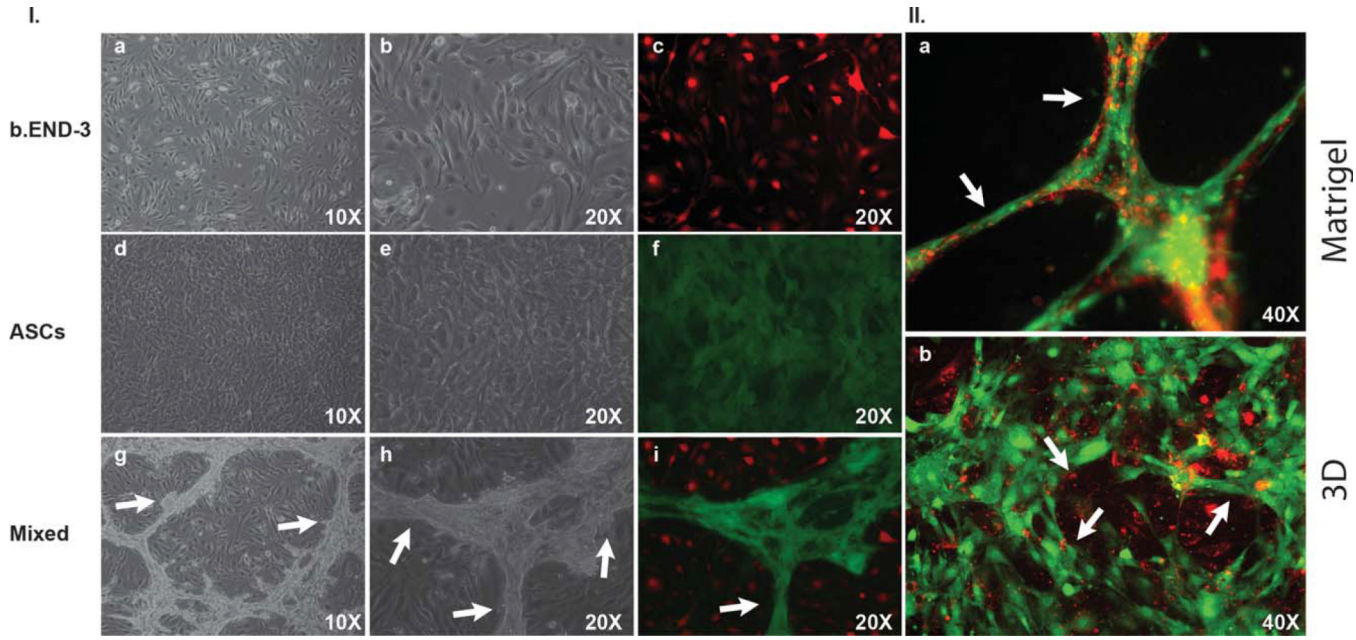

FIGURE 3.

Representative light and fluorescent microscopy images of ASCs, and b.END-3 cells when co-cultured or seeded alone on Matrigel or on 3D polystyrene substrate. Image of ASCs and b.END-3 on day 3 in the culture alone, demonstrating the absence of any well-formed tubular network l(a–f). Fluorescence microscopy images of GFP^+ ASCs (green) co-seeded with PKH26-labeled b.END-3 cells (red) on Matrigel under normal conditions l(i). High magnification merged images show ASCs and b.END-3 cells working cooperatively in the formation of branching l(i). Completely lumenized tubular structrures develop *in vitro* in Matrigel 11(a). Note that the lumen is free of GFP^+ and PKH26 signal 11(a). ASCs were seeded at a concentration of 1×10^5 cells per well of 12-well plates and incubated for 72 h at 37°C in 5% $C0_2$. White arrows indicate tubule formation. Fluorescent microscopy of 3D scaffolds showing the 3D network of cell aggregates within the scaffold ll(b) arrows indicate lumen with ASCs contribute to *in vitro* formation of a 3D pre-vascular network within a porous scaffold. [Color figure can be viewed in the online issue, which is available at wileyonlinelibrary.com.]

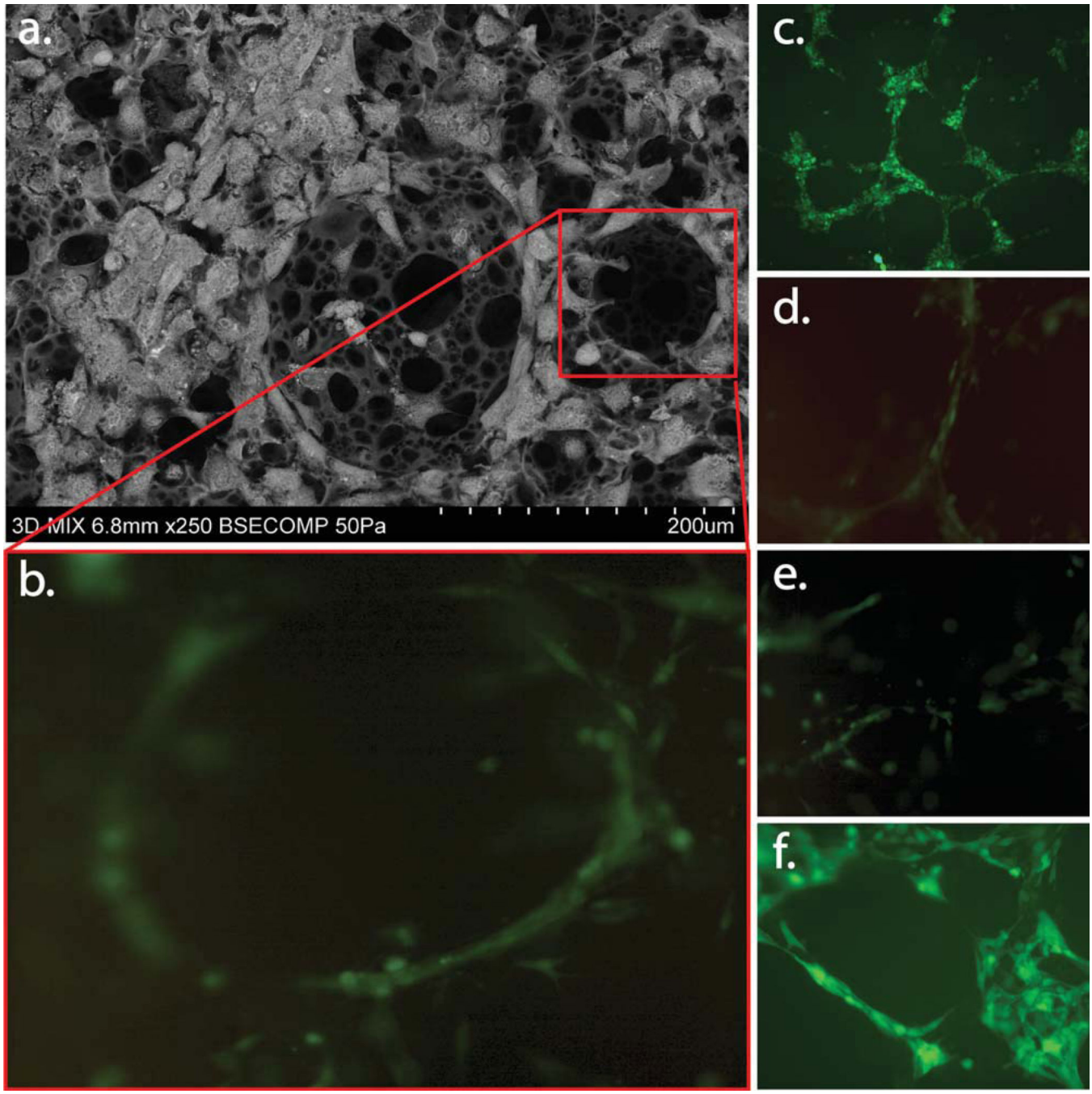

FIGURE 4.

Fluorescent microscopy of 3D scaffolds showing the 3D network of cell aggregates within the scaffold arrows indicate lumen with ASCs contribute to *in vitro* formation of a 3D pre-vascular network within a porous scaffold as seen in (c–f). SEM depicting organization and pro-iferation of ASCs, and b.END-3 cells when co-cultured on 3D polystyrene substrate (a). Physical interaction of ASCs with b.END-3 network formed in the 3D scaffold at 3 days post seeding. Confocal fluorescent images in (c–f) are cross-section projections at the surface (c) 60 μm, (d) 120 μm, (e) and 170 μm (f) within the polystyrene scaffolds. The

penetration of the ASCs cells within the porous structures forming pre-capillary-like structures similar to the ones seen in matrigel control [Fig. 3(b,i)]. [Color figure can be viewed in the online issue, which is available at wileyonlinelibrary.com.]

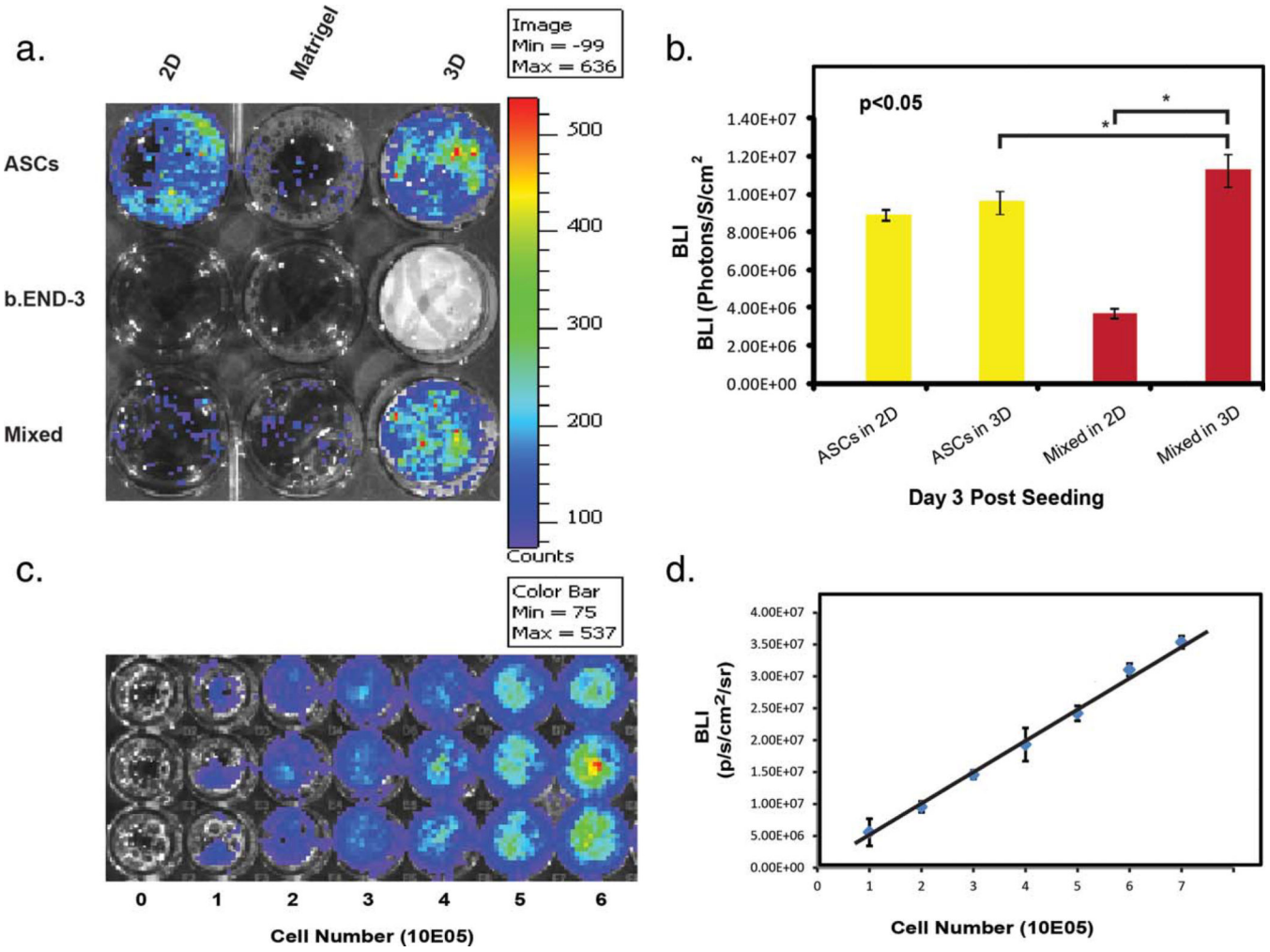

FIGURE 5.

Bioluminescent images of 1×10^5 of ASCs, b.END-3 and co-cultures of ASCs (0.5×10^5) with b.END-3 cells (0.5×10^5) seeded onto 2D, 3D Polystyrene substrates, or Matrigel at 3 days post-seeding (a). Bioluminescent imaging of co-cultured substrates showed increased bioluminescence compared to undifferentiated ASCs seeded onto the 2D substrates (b). Firefly luciferase signal of ASCs-hFluc-hrGFP cells at different cell numbers (c). Calibration curve from *in vitro* imaging analysis of stably transduced ASCs. Linear correlation of cell numbers and bioluminescence imaging (BLI) signals (photons per s per cm^2 per steridian) in (a) ($r^2 = 0.99$) (d). This positive correlation between cell number and bio-luminescent signal confirms the quantitative ability of bioluminescence imaging for tracking cell proliferation. Images were taken at the time points indicated. Experiments were performed in triplicate. The error bars indicate SD (*$p < 0.05$). [Color figure can be viewed in the online issue, which is available at wileyonlinelibrary.com.]

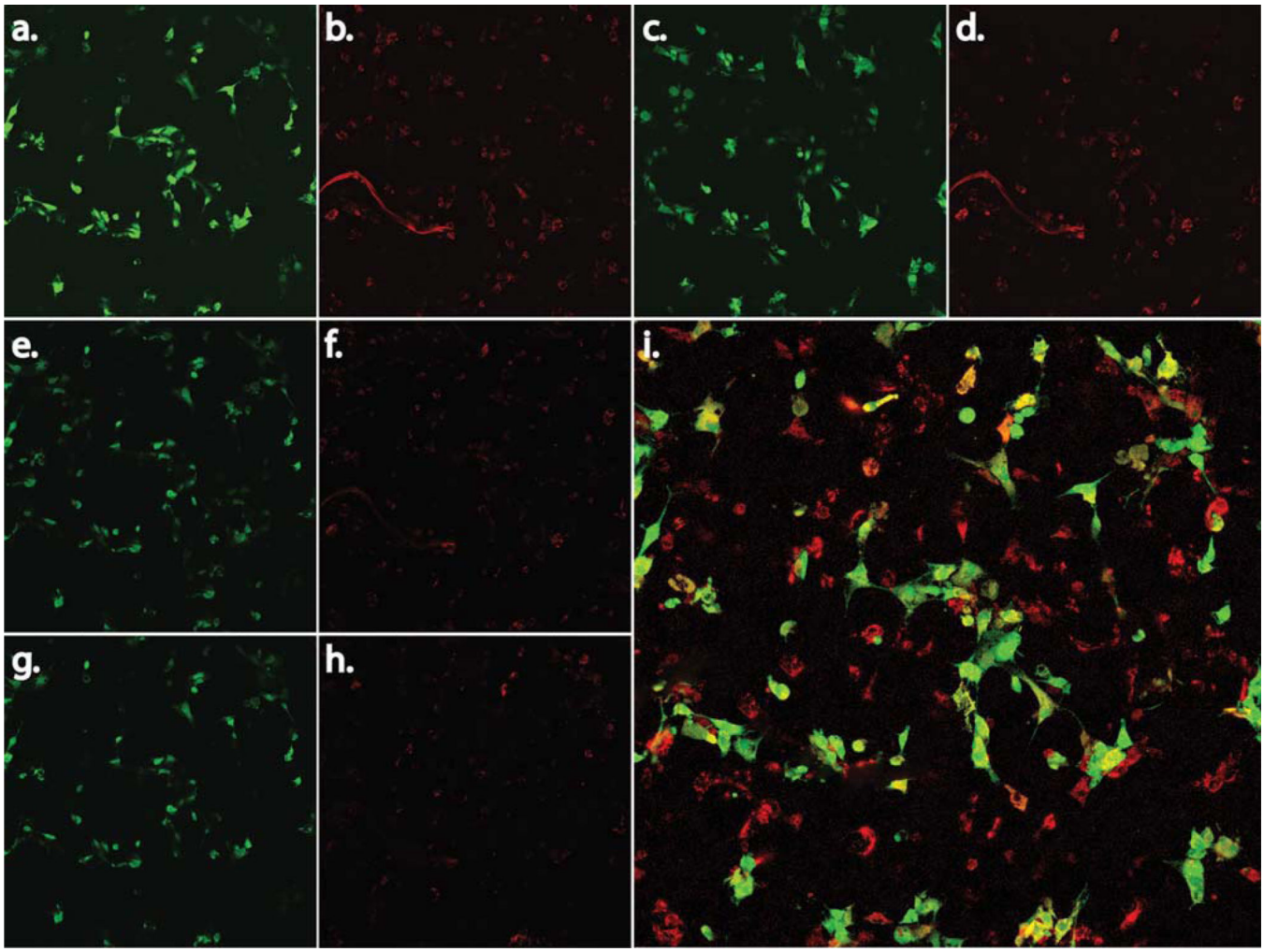

FIGURE 6.

Confocal microscopy analysis within longitudinal sections of the 3D polystyrene substrate that have co-cultures of GFP^+ ASCs (0.5×10^5) and PKH26-labelled murine b.END-3 cells (0.5×10^5). Interactions between ASCs, and b.END-3 are shown throughout the Serial confoca sections (a–h) providing an extra perspective of the growth and adhesion of the two cell lines within the 3D substrate. Serial confocal sections began 10 m in from the top surface (a) (top left panel) and ended 200 μm in from the bottom (h). Confocal microscope images show the cells entering the outermost layer of pores. The seeding surface is seen in the upper parts of the images. Overview of a scaffold where there was a wide band of cells on top of the material (i). [Color figure can be viewed in the online issue, which is available at wileyonlinelibrary.com.]

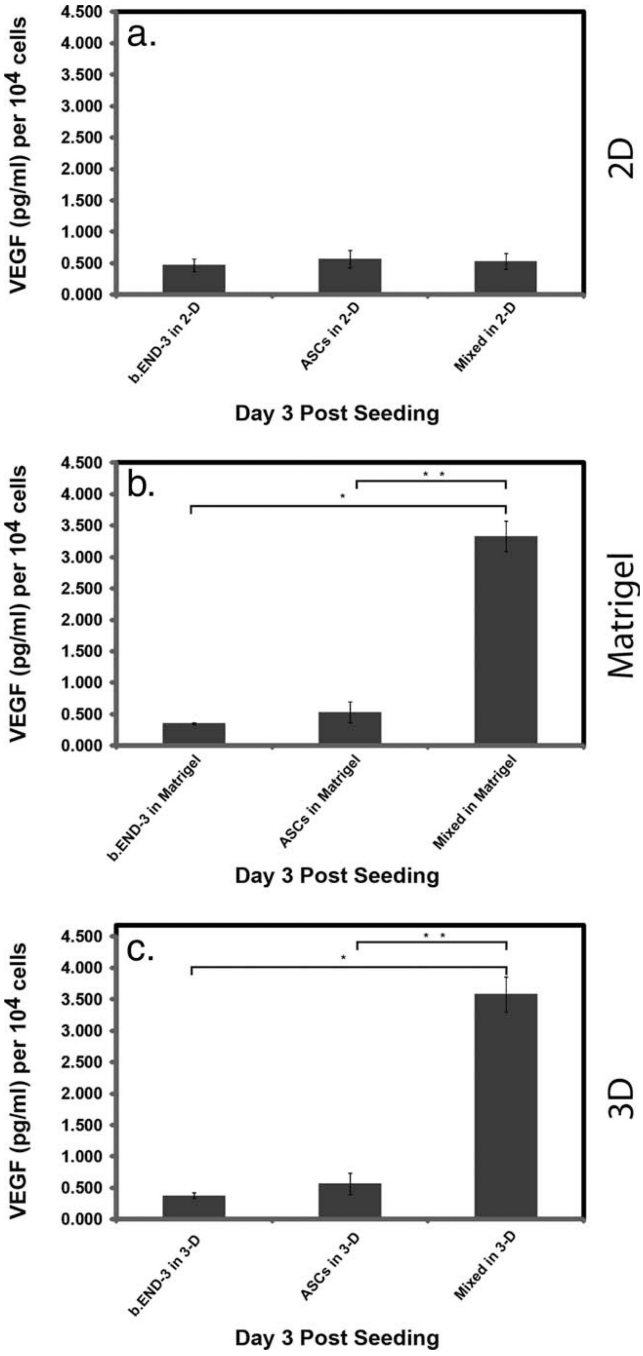

FIGURE 7.

VEGF ELISA results for supernatants of ASCs, b.END-3 and co-cultures. Cells were seeded onto 2D (a) and 3D (c) polystyrene or Matrigel (b) and cultured for 72-h under normoxic conditions. Significantly higher levels of VEGF were seen in co-cultures of ASCs, and b.END-3 when compared to controls. Triplicate measurements were performed and the data are from a representative experiment. Data are presented as mean ± SEM. VEGF levels were

normalized to the number of cells at the time of seeding, expressed as pg/mL per 10^6 cells. *$p < 0.05$.